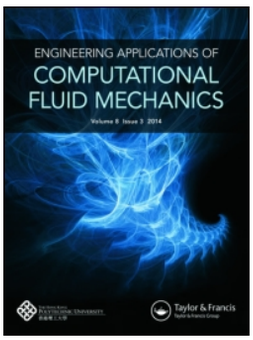

Taylor & Francis
Taylor & Francis Group

Engineering Applications of Computational Fluid Mechanics

ISSN: 1994-2060 (Print) 1997-003X (Online) Journal homepage: http://www.tandfonline.com/loi/tcfm20

Actuator disc methods for open propellers: assessments of numerical methods

R. Bontempo & M. Manna

To cite this article: R. Bontempo & M. Manna (2017) Actuator disc methods for open propellers: assessments of numerical methods, Engineering Applications of Computational Fluid Mechanics, 11:1, 42-53, DOI: 10.1080/19942060.2016.1234978

To link to this article: http://dx.doi.org/10.1080/19942060.2016.1234978

Published online: 20 Oct 2016.

ENGINEERING APPLICATIONS OF COMPUTATIONAL FLUID MECHANICS, 2017
VOL. 11, NO. 1, 42–53
http://dx.doi.org/10.1080/19942060.2016.1234978

Taylor & Francis
Taylor & Francis Group

Actuator disc methods for open propellers: assessments of numerical methods

R. Bontempo and M. Manna

Department of Industrial Engineering, University of Naples Federico II, Naples, Italy

ABSTRACT

The paper describes the assessment of two different actuator disc models as applied to the flow around open propellers. The first method is based on a semi-analytical approach returning the solution for the nonlinear differential equation governing the axisymmetric, steady, inviscid and incompressible flow around an actuator disc. Despite its low computational cost, the method does not require simplifying assumptions regarding the shape of the slipstream, e.g. the wake contraction is not disregarded or prescribed in advance. Moreover, the presence of a tangential velocity in the wake as well as the spanwise variation of the load are taken into account. The second one is a commonly used procedure based on CFD techniques in which the effects of the propeller are synthetically described through a set of body forces distributed over the disc surface. Both methods avoid the difficulties and the computational costs associated with the resolution of the propeller blades geometrical details. The comparison is based on an in-depth error analysis of the two procedures which results in a set of reference data with controlled accuracy. An excellent agreement has been documented between the two methods while the computational complexity is obviously very different. Among other things the comparison is also aimed at verifying the accuracy of the semi-analytical approach at each point of the computational domain and at quantifying the effect of the errors embodied in the two methods on the quality of the solution, both in terms of global and local performance parameters. Furthermore, the paper provides a set of reference solutions with controlled accuracy that could be used for the verification of new and existing computational methods. Finally, the computational cost of the semi-analytical model is quantified, thus providing a valuable information to designers who need to select a cost effective and reliable analysis tool.

ARTICLE HISTORY
Received 6 March 2016
Accepted 7 September 2016

KEYWORDS
Actuator disc; nonlinear actuator disc; CFD actuator disc; propellers

1. Introduction

The 'actuator disc method' (ADM) constitutes a widely employed design and/or analysis tool both in its analytical and CFD-based formulation. Besides the most famous and simple momentum theory (Glauert, 1935), a nonlinear variant of the actuator disc model has also been developed by Wu (1962) in his pioneering work. Since then Greenberg and Powers (1970) and Greenberg (1972) provided important improvements to the nonlinear ADM both in its theoretical and numerical aspects, and a detailed review of the most relevant analytical matters can be found in the book of Breslin and Andersen (1994).

More recently, Conway (1998) provided an exact and implicit solution to the flow around an actuator disc. The solution can be regarded as the flow induced by a distribution of ring vortices modelling the propeller wake. The solution is made explicit through an iterative and semi-analytical procedure, and, for this reason, the method will be termed the 'semi-analytical actuator disc method' (SA-ADM) from here on. The method deals with rotors characterized by heavy loads with non-uniform distributions and with slipstream rotation and contraction.

Recently, the SA-ADM has also been generalized to ducted rotors (see Bontempo, Cardone, & Manna, 2016; Bontempo, Cardone, Manna, & Vorraro 2014, 2015a, 2015b; Bontempo & Manna, 2013, 2014, 2016b, 2016c, 2016d). Moreover, it has also been employed to evaluate the errors embodied in the axial and general momentum theory (Bontempo & Manna, 2016a).

Finally, it should be mentioned that all actuator disc models, like the SA-ADM, are representative of a rotor with infinite blades. Thus, the flow nonuniformity due to the presence of the blades and tip loss effects are not directly taken into account. However, these phenomena could be modelled through empirical or theoretical models (Shen, Sørensen, & Mikkelsen, 2005).

Nowadays, CFD methods have a predominant role in most fluid dynamics applications (Bellary et al., 2016; Das et al., 2015; Fu, Uddin, & Curley, 2015; Greifzu, Kratzsch,

CONTACT R. Bontempo rodolfo.bontempo@unina.it

Forgber, Lindner, & Schwarze, 2015; Hu, Li, Han, Cai, & Xu, 2016; Insinna, Griffini, Salvadori, & Martelli, 2014; Liu et al., 2015; Luo, Yu, Dai, Fang, and Fan, 2016; Manna, Benocci, & Simons, 2005; Manna, Vacca, & Deville, 2004; Montis et al., 2009; Shi, Xu, & Wei, 2016; Sun, Su, Wang, & Hu, 2016). CFD techniques are also widely employed to solve the Reynolds averaged Navier–Stokes (RANS) or Euler equations in a domain comprising a propeller that is represented through a body-force distribution over a disc area. For this reason we name this approach the 'CFD actuator disc method' (CFD-ADM). The main goal of this technique is to reduce the computational efforts related to the solution of the flow around the propeller blades. Moreover, since the screw is replaced by a simple disc, mesh generation efforts are greatly reduced. Obviously, such a method cannot predict the details of the flow around the rotor and the blades tip, but it can successfully address the global effects of the propeller on the hull flow, as witnessed by the short literature review reported hereafter.

At the end of the 1970s, Schetz and Favin (1977, 1979) attempted to represent the propeller through an axisymmetric distribution of body forces weakly coupled to the incompressible RANS equations. Kawamura, Miyata, and Mashimo (1997) simulated the flow around five tanker hulls introducing the Nakatake (1989) simplified actuator disc propeller model into the WISDAM-V finite-volume method developed by Miyata, Zhu, and Watanabe (1992). In the above procedure, the interaction between the two flow models is handled through a time-marching procedure which should converge towards the steady self-propelling condition. Phillips, Turnock, and Furlong (2009) developed a coupled blade element–RANS procedure to determine the manoeuvring coefficients of a self-propelled ship hull travelling straight ahead. The analysis was carried out at a prescribed drift angle and for differing rudder angles. In their approach, the blade element method is used to model the effects of the propeller with a set of forces which are then inserted into the RANS domain. The latter may include the ship hull and the rudder. A circumferentially averaged nominal wake fraction is evaluated with a RANS code at different radial stations. The computed wake velocity is used to evaluate the propeller loads through the blade element method. Then, the calculated thrust and torque values are introduced in the CFD code as momentum sources distributed over a disc of finite thickness. This procedure is repeated until convergence.

Choi, Min, Kim, Lee, and Seo (2010) examined the speed–power performance of various types of commercial ship hulls analysing their resistance and propulsion characteristics. In their study asymmetric body forces are used, while the effect of a finite number of blades is neglected. The adopted procedure starts by first evaluating the incoming flow velocity at the propeller plane by the commercial RANS solver ANSYS® Fluent®. Then, the obtained inflow is used as input data for a potential-flow solver. After that the thrust and torque distributions on the actuator disc plane are represented as known body forces in the RANS code by means of a 'user-defined function' (UDF). Obviously, the procedure is iterated until convergence. The UDF is a technique that allows any user to implement certain models into the general multi-purpose ANSYS® Fluent® code. In that context the UDF was used to insert the asymmetric body-force propeller model into the CFD code. Starke and Bosschers (2012) adopted an hybrid boundary element method-RANS approach to investigate the scale effects in ship powering performance. The viscous flow around the ship hull is coupled with the flow induced by the screw modelled with a boundary element method. Moreover, an extensive description of the coupling procedure details is also reported. In order to predict the free turning manoeuvre of a tanker-like ship, Broglia, Dubbioso, Durante, and Di Mascio (2013) coupled different propeller actuator disc models with an in-house developed URANS code. Two models were considered: a modified Hough and Ordway (1964) approach and a model based on blade element momentum theory.

Finally, it should be mentioned that the CFD-ADM is a method that is also widely employed in the wind turbine technology field (see for instance Masson, Ammara, & Paraschivoiu, 1997; Mikkelsen, Sørensen, & Shen, 2001; Hansen, Sørensen, Voutsinas, Sørensen, & Madsen, 2006; Shen et al., 2005; Sørensen, 2011; Sørensen & Kock, 1995; Sørensen, Shen, & Munduate, 1998; Troldborg, Sørensen, Réthoré, & van der Laan, 2015).

The literature review presented above proves that the ADM is currently and successfully employed to study propeller wakes. This paper, which relies on the work of Conway (1998), quantifies the effect of the errors embodied in the SA-ADM and CFD-ADM on the quality of the solution, both in terms of global and local performance parameters. A code-to-code comparison has been carried out with the objective of establishing the computational cost required by the two methods to comply with a prescribed accuracy in the clean context offered by the selected test cases. In addition to what has just been described, further original contributions of the paper can be found. For example, the comparison is also aimed at verifying the accuracy of the SA-ADM at each point of the computational domain, not only in the far wake as previously reported in Conway (1998). Furthermore, the paper provides a set of reference solutions with controlled accuracy that could be used for the verification of new and existing computational methods. Finally, the

computational cost associated with the SA-ADM method is quantified; a fact of the utmost importance for designers who have to select the optimal analysis tool to be integrated in a design system.

The paper is structured as follows. Section 2 comprises a synthesis of the semi-analytical actuator disc of Conway (1998), aimed at pointing out the most important numerical issues discussed in the forthcoming error analysis. Then, the SA-ADM and CFD-ADM results are compared in Section 3. With this aim, the popular CFD suite ANSYS® Fluent® is adopted.

2. The SA-ADM

Consider a cylindrical coordinate system (ζ, σ, θ). The actuator disc centre is located at (0,0,0), its radius is σ_{ad} and the velocity of the free stream is U_∞ (see Figure 1). Suppose the flow to be axisymmetric, steady, incompressible and inviscid. Since the flow is axisymmetric, the Stokes stream function Ψ, defined as

$$u = \frac{1}{\sigma}\frac{\partial \Psi}{\partial \sigma} \qquad v = -\frac{1}{\sigma}\frac{\partial \Psi}{\partial \zeta}, \tag{1}$$

can be conveniently introduced. In the above equation, the velocity vector is $\boldsymbol{u} = (u, v, w)$. Moreover, for the class of axisymmetric problems the vorticity vector reads

$$\boldsymbol{\omega} = (\omega_\zeta, \omega_\sigma, \omega_\theta) = \left(\frac{1}{\sigma}\frac{\partial(\sigma w)}{\partial \sigma}, -\frac{\partial w}{\partial \zeta}, \frac{\partial v}{\partial \zeta} - \frac{\partial u}{\partial \sigma}\right). \tag{2}$$

Furthermore, by means of Equation (1), the θ-component of the vorticity can be written as

$$\frac{\partial^2 \Psi}{\partial \sigma^2} - \frac{1}{\sigma}\frac{\partial \Psi}{\partial \sigma} + \frac{\partial^2 \Psi}{\partial \zeta^2} = -\omega_\theta \sigma. \tag{3}$$

Note that the minus sign in the first-order derivative term makes the above equation different from the well-known axisymmetric formulation of the Poisson equation in cylindrical coordinates. Using the momentum and the angular momentum equations (Wu, 1962), the above Equation (3) returns

$$\frac{\partial^2 \Psi}{\partial \sigma^2} - \frac{1}{\sigma}\frac{\partial \Psi}{\partial \sigma} + \frac{\partial^2 \Psi}{\partial \zeta^2} = -\omega_\theta \sigma = \begin{cases} \dfrac{\Omega^2 \sigma^2 - \mathcal{H}}{\Omega^2}\dfrac{\mathrm{d}\mathcal{H}}{\mathrm{d}\Psi} & \text{inside the slipstream,} \\ 0 & \text{outside the slipstream.} \end{cases} \tag{4}$$

This is the partial and nonlinear differential equation that governs the through-flow across the device. In particular, Ω is the angular velocity, while the load distribution $\mathcal{H}$ is defined as

$$\mathcal{H}(\Psi) = \Delta H_{\text{across the disc}} = H(\Psi)|_{(\zeta > 0, \sigma < \sigma_s(\zeta))} - H_\infty.$$

In the above equation, $H = p/\rho + (u^2 + v^2 + w^2)/2$ is the Bernoulli constant and $\sigma_s(\zeta)$ is the slipstream location defining the radial extension of the wake as a function of the streamwise coordinate ζ. Thus, the wake is mathematically defined as the space region $\{(\zeta, \sigma) \in \mathbb{R} \times \mathbb{R} : \zeta > 0, \sigma < \sigma_s(\zeta)\}$. The conditions at infinity that have to be associated with Equation (4) are (Wu, 1962):

$$\frac{1}{\sigma}\frac{\partial \Psi}{\partial \sigma} \to U_\infty, \qquad \frac{\partial \Psi}{\partial \zeta} \to 0 \quad \text{as } \zeta \to -\infty \text{ or } \sigma \to \infty, \tag{5a}$$

$$\frac{\partial \Psi}{\partial \zeta} \to 0 \quad \text{as } \zeta \to +\infty. \tag{5b}$$

The Stokes stream function definition (1) can be easily employed to clarify the meaning of the previous conditions. From Equation (4) it is easily understood that, to formulate the differential problem (4)–(5) completely, two key physical quantities, i.e. the angular velocity Ω (or the advance coefficient J) and the distribution of the

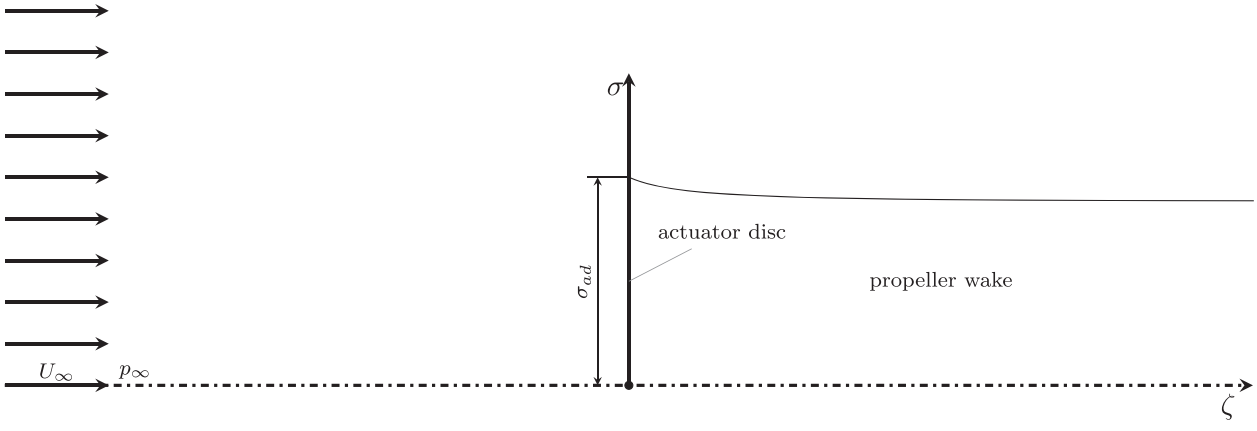

Figure 1. Schematic view of the actuator disc configuration.

load, have to be known in advance. Indeed the function $\sigma_s(\zeta)$, defining the wake shape, is not known beforehand and it has to be computed through the iterative method detailed in Section 2.2. Eventually, as soon as the (u, v) components of the velocity field have been obtained, the tangential velocity component w can be evaluated by the well-known angular momentum equation

$$\mathcal{H}(\Psi) = H(\Psi) - H_\infty = \Omega\sigma w. \tag{6}$$

2.1. Exact solution of the flow around an actuator disc

As thoroughly described in Conway (1998) and the references therein, the flow around an actuator disc is modelled with the help of ring vortices (see Figure 2). In more detail, the stream function and the velocity field (u', v') associated with a single ring vortex of radius r, strength κ and located at $\zeta = z$ and $\sigma = 0$, are (Basset, 1888; Lamb, 1932)

$$\frac{\Psi'(\zeta,\sigma)}{\sigma} = \frac{\kappa r}{2}\int_0^\infty \mathrm{e}^{-s|\zeta-z|}\mathrm{J}_1(sr)\mathrm{J}_1(s\sigma)\,\mathrm{d}s, \tag{7}$$

$$u'(\zeta,\sigma) = \frac{\kappa r}{2}\int_0^\infty \mathrm{e}^{-s|\zeta-z|}s\mathrm{J}_1(sr)\mathrm{J}_0(s\sigma)\,\mathrm{d}s, \tag{8}$$

$$v'(\zeta,\sigma) = \pm\frac{\kappa r}{2}\int_0^\infty \mathrm{e}^{-s|\zeta-z|}s\mathrm{J}_1(sr)\mathrm{J}_1(s\sigma)\,\mathrm{d}s, \tag{9}$$

where for $\zeta - z \geq 0$ the positive sign holds and vice versa. The quantity J, appearing in the above equation, represents a Bessel function of the first kind. The solution for Ψ can be written as the superposition of the flow induced by a distribution of ring vortices modelling the propeller wake. The density strength of this distribution is named $\gamma_{\mathrm{ad}}(\zeta,\sigma)$, where the subscript 'ad' stands for 'actuator disc', meaning that the ring vortices are used to describe the flow induced by the disc. The exact flow solution is then obtained by integrating Equation (7) over the wake, i.e. (Conway, 1998)

$$\frac{\Psi(\zeta,\sigma)}{\sigma} = \frac{1}{2}\int_0^\infty\int_0^{\sigma_s(z)}\int_0^\infty \mathrm{e}^{-s|\zeta-z|}\gamma_{\mathrm{ad}}(z,r)r\mathrm{J}_1(sr) \times \mathrm{J}_1(s\sigma)\,\mathrm{d}s\,\mathrm{d}r\,\mathrm{d}z + \frac{U_\infty\sigma}{2}. \tag{10}$$

Specifically, the first term in Equation (10) represents the flow promoted by the actuator disc, whilst the second term is the flow induced by the free stream.

Consider now the requirements that must be met by $\gamma_{\mathrm{ad}}(\zeta,\sigma)$ so that Equation (10) can be regarded as the solution of the differential problem (4)–(5). As previously stated, the distribution of the load and the advance coefficient have to be preliminarily prescribed. Moreover, these two physical quantities are directly related to the tangential vorticity distribution in the wake through Equation (4). This means that the actuator disc ring vortex distribution, i.e. the density strength $\gamma_{\mathrm{ad}}(\zeta,\sigma)$ appearing in Equation (10), has to reproduce the prescribed wake vorticity field $\omega_\theta(\zeta,\sigma)$ induced by the disc $\mathcal{H}(\Psi)$ distribution (see Equation 4). Note that, for the through-flow field $(u, v, 0)$, ω_θ is the only vorticity component that is different from zero, and the vorticity strength vector of a ring vortex is also directed in the θ-direction (see Figure 2). From these considerations it can be easily inferred that the following equation must hold: $\gamma_{\mathrm{ad}}(\zeta,\sigma) = \omega_\theta(\zeta,\sigma)$ (see Conway, 1998). The conditions at infinity (5a) and (5b) are obviously satisfied by the overall flow solution (10). Finally, integrating Equations (8) and (9) over the wake space region, the disc induced velocities u_{ad} and v_{ad} read

$$u_{\mathrm{ad}}(\zeta,\sigma) = \frac{1}{2}\int_0^\infty\int_0^{\sigma_s(z)}\int_0^\infty \mathrm{e}^{-s|\zeta-z|}\gamma_{\mathrm{ad}}(z,r)sr\mathrm{J}_1(sr) \times \mathrm{J}_0(s\sigma)\,\mathrm{d}s\,\mathrm{d}r\,\mathrm{d}z, \tag{11}$$

$$v_{\mathrm{ad}}(\zeta,\sigma) = \pm\frac{1}{2}\int_0^\infty\int_0^{\sigma_s(z)}\int_0^\infty \mathrm{e}^{-s|\zeta-z|}\gamma_{\mathrm{ad}}(z,r)sr \times \mathrm{J}_1(sr)\mathrm{J}_1(s\sigma)\,\mathrm{d}s\,\mathrm{d}r\,\mathrm{d}z. \tag{12}$$

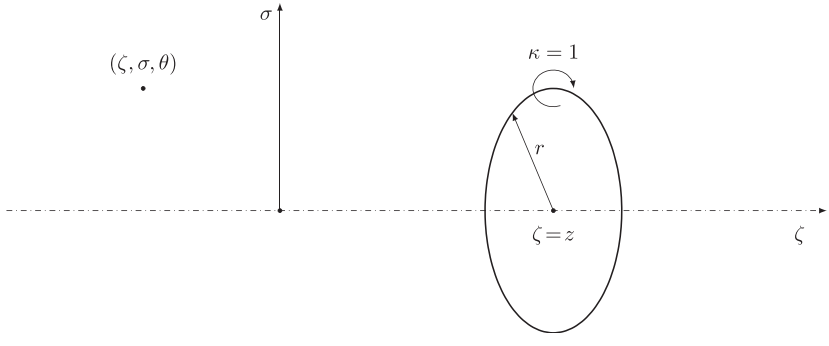

Figure 2. Schematic view of the ring vortex employed to model the flow around an actuator disc.

2.2. SA-ADM: solution strategy

As stated in the previous subsection, Equation (10) is the exact solution of the through-flow around an actuator disc. However, the implicitness of this expression prevents the direct evaluation of Ψ via (10), the unknowns $\sigma_s(\zeta)$ and $\gamma_{\mathrm{ad}}(\zeta,\sigma)$ depending upon the Stokes stream function. The computation of Ψ is then carried out through an iterative and semi-analytical procedure thoroughly detailed in Conway (1998) and summarized hereinafter. Some improvements in the numerical approach are also introduced.

As detailed in Conway (1998), the method can deal with an $\mathcal{H}$ distribution of the polynomial type

$$\mathcal{H}(\Psi)=\sum_{m=0}^{M} a_m\left(\frac{\Psi}{\Psi_{\sigma_{\mathrm{ad}}}}\right)^m, \tag{13}$$

where the Ψ value at $(\zeta=0,\sigma=\sigma_{\mathrm{ad}})$ is termed $\Psi_{\sigma_{\mathrm{ad}}}$. If $\mathcal{H}(\Psi)$ is supposed to be C^1 continuous then, from Equations (13) and (4), ω_θ can be written as

$$\frac{\omega_\theta(\zeta,\sigma)}{\sigma}=\left[\frac{J^2}{\pi^2U_\infty^2}\left(\frac{\sigma_{\mathrm{ad}}}{\sigma}\right)^2\sum_{m=0}^{M} a_m\left(\frac{\Psi}{\Psi_{\sigma_{\mathrm{ad}}}}\right)^m-1\right]\times\sum_{m=1}^{M}\frac{ma_m}{\Psi_{\sigma_{\mathrm{ad}}}}\left(\frac{\Psi}{\Psi_{\sigma_{\mathrm{ad}}}}\right)^{m-1}. \tag{14}$$

In order to integrate Equations (10)–(12) exactly, the tangential vorticity, appearing on the left-hand side of Equation (14), can conveniently be expressed through the following polynomial expansion (Conway, 1998):

$$\frac{\omega_\theta(\zeta,\sigma)}{\sigma}=\sum_{n=0}^{N}A_n(\zeta)\left[1-\left(\frac{\sigma}{\sigma_s(\zeta)}\right)^2\right]^n. \tag{15}$$

In fact, with the help of this alternative ω_θ form, the radial integral in Equations (10)–(12) can be exactly evaluated, thus obtaining

$$\Psi(\zeta,\sigma)=\sigma\int_0^\infty\sum_{n=0}^{N}A_n(z)2^{n-1}n!\sigma_s^{2-n}(z)\times I_{(-(n+1),n+2,1)}(\sigma_s(z),\sigma,\zeta-z)\,\mathrm{d}z+\frac{U_\infty\sigma^2}{2}, \tag{16}$$

$$u_{\mathrm{ad}}(\zeta,\sigma)=\int_0^\infty\sum_{n=0}^{N}A_n(z)2^{n-1}n!\sigma_s^{2-n}(z)\times I_{(-n,n+2,0)}(\sigma_s(z),\sigma,\zeta-z)\,\mathrm{d}z, \tag{17}$$

$$v_{\mathrm{ad}}(\zeta,\sigma)=\pm\int_0^\infty\sum_{n=0}^{N}A_n(z)2^{n-1}n!\sigma_s^{2-n}(z)\times I_{(-n,n+2,1)}(\sigma_s(z),\sigma,\zeta-z)\,\mathrm{d}z. \tag{18}$$

The quantities

$$I_{(\xi,\mu,\nu)}=\int_0^\infty \mathrm{e}^{-s|\zeta-z|}s^\xi \mathrm{J}_\mu(sr)\mathrm{J}_\nu(s\sigma)\,\mathrm{d}s, \tag{19}$$

which appear in the above three equations, can be evaluated through recursive relations for each value of the integers ξ, μ and ν (see Bontempo, 2014).

In order to integrate Equations (16)–(18), a further difficulty has to be tackled. In fact the function $\sigma_s(\zeta)$ describing the shape of the wake is still unknown and must be determined as part of the whole solution. One way to proceed is as follows. Firstly, on account of the fact that the Stokes stream function is constant on the wake edge, one can exploit Equation (16) at $\sigma_s(\zeta)$. By doing so, an integral equation for $\sigma_s(\zeta)$ is obtained:

$$\Psi(0,\sigma_{\mathrm{ad}})=\frac{U_\infty\sigma_s^2(\zeta)}{2}+\sigma_s(\zeta)\int_0^\infty\sum_{n=0}^{N}A_n(z)2^{n-1}n!\times\sigma_s^{2-n}(z)I_{(-(n+1),n+2,1)}\times(\sigma_s(z),\sigma_s(z),\zeta-z)\,\mathrm{d}z. \tag{20}$$

At this point the solution procedure can be outlined as follows.

(1) Assume that provisional values of the discrete counterparts of the $\sigma_s(\zeta)$ and $\{A_n(\zeta)\}_{n=0,N}$ distributions are known for n_z values of the axial coordinate.
(2) Then replace the continuous Ψ and ω_θ distributions with their discrete representations on a grid spanning the wake with $n_{zs}\times n_{rs}$ points in the axial and radial directions, respectively. Specifically, integrate Equation (16) in the axial direction with an adaptive quadrature scheme to obtain the discrete Ψ distribution at all mesh points. Moreover, with the help of Equation (14) the azimuthal component of the vorticity can also be evaluated at all mesh points.
(3) A least-squares minimization procedure is then applied to parametrize the ω_θ distributions, computed at the previous step, leading to a new set of $\{A_n(\zeta)\}_{n=0,N}$.
(4) Update the slipstream $\sigma_s(\zeta)$ from Equation (20) evaluated at $(\zeta,\sigma_s(\zeta))$.
(5) Go to item (1) until convergence of the slipstream $\sigma_s(\zeta)$ is reached.

The unknowns $\sigma_s(\zeta)$ and Ψ are initialized neglecting the presence of the disc. Note that, in comparison to previously proposed implementations of the method (Conway, 1998; Greenberg & Powers, 1970), in the actual version of the semi-analytical procedure there is no need to approximate the updated slipstream shape $\sigma_s(\zeta)$ (see

point (4)) through a least-squares approach. By so doing, the accuracy of the solution is improved further.

In the following, the SA-ADM is employed to simulate the flow around a propeller with $J = 0.5$ and characterized by a parabolic versus Ψ load distribution, i.e. $M = 2$ in Equation (13). From the same Equation (13), it can be readily understood that $\mathcal{H}(0) = a_0$. Moreover, in order to enforce a vanishing load at the disc edge and at the centre, the following two conditions have to be satisfied: $a_0 = 0$ and the sum of the a_m parameters for $m = 1, \ldots, M$ has also to be zero, i.e. $\Sigma_{m=1}^{M} a_m = 0$. Thus, for a parabolic distribution of the load, $a_0 = 0$, $a_1 = -a_2$ and

$$\mathcal{H}(\Psi) = a_1 \left[\frac{\Psi}{\Psi_{\sigma_{\text{ad}}}} - \left(\frac{\Psi}{\Psi_{\sigma_{\text{ad}}}} \right)^2 \right] = \frac{U_\infty \Psi_{\sigma_{\text{ad}}} \hat{b}}{\sigma_{\text{ad}}^2} \left[\frac{\Psi}{\Psi_{\sigma_{\text{ad}}}} - \left(\frac{\Psi}{\Psi_{\sigma_{\text{ad}}}} \right)^2 \right], \qquad (21)$$

where $\hat{b} = \sigma_{\text{ad}}^2 a_1 / (U_\infty \Psi_{\sigma_{\text{ad}}})$.

3. Comparison between the SA-ADM and the CFD-ADM

As discussed in the introduction, the CFD-ADM is a commonly employed analysis method that provides the solution of the Navier–Stokes or Euler equations in a domain comprising a propeller represented through a body-force distribution acting over a disc area. From a computational point of view, these distributions are obtained by pursuing several approaches, such as iterative and interactive coupling with lifting-surface, boundary element or blade element methods. However, many researchers have often applied a prescribed body-force distribution over the disc area (see for instance Dai, Gorski, & Haussling, 1991; Hoekstra, 2006; Piquet, Queutey, & Visonneau, 1987; Yang, Hartwich, & Sundaram, 1991). In this paper a CFD-ADM method is implemented in the popular CFD suite Fluent® by introducing source terms in the axial and tangential momentum equations. In the following section, the results obtained by modelling the rotor through the CFD-ADM are compared with those of the semi-analytical procedure described in Section 2, assuming identical body-force distributions. To this end, an error analysis is conducted for both methods in Sections 3.1 and 3.2. Finally, in Section 3.3 a detailed comparison between the results of the two procedures is carried out.

3.1. Analysis of the error for the SA-ADM

As reported in Conway (1998), the evaluation of the Stokes stream function Ψ via the exact solution of the governing equation (10) is prevented due to the implicitness of this equation. In particular, the slipstream location σ_s and the density strength γ_{ad} all depend upon Ψ. The solution can be made explicit through the semi-analytical procedure developed by Conway (1998) and further improved by Bontempo and Manna (2013, 2014). As detailed in Section 2.2, this procedure introduces three numerical parameters, i.e. n_z, n_{zs}, n_{rs}, whose effects on the solution are investigated in the following error analysis. In addition to these parameters, the effects of some other numerical quantities are also investigated. One of these is the error related to the numerical integration of Equations (16)–(18). This task is accomplished with the help of an adaptive quadrature scheme (Lyness, 1970), which allows a required tolerance value (*quad_err* in Table 1) to be prescribed in advance. Another numerical parameter is the degree N of the polynomial appearing on the right-hand side of Equation (15). Finally, the last numerical parameter involved in the semi-analytical process is the value of the residue *res* which has to be achieved to exit the iterative procedure. The residue is defined in terms of two consecutive slipstream radii evaluated at $\zeta = 15\sigma_{\text{ad}}$:

$$\text{res}^n = \frac{|\Delta\sigma_s(\zeta = 15\sigma_{\text{ad}})|}{\sigma_{\text{ad}}} = \frac{|\sigma_s^n - \sigma_s^{n-1}|}{\sigma_{\text{ad}}}.$$

For the sake of conciseness, all numerical parameters are simultaneously made to increase in a six-level range as shown in Table 1. Assuming case SA–6 of Table 1 as reference, the relative errors on the performance coefficients and the discrete L^2 errors for u are reported in Table 2. The following classical definitions are adopted for the performance coefficients:

$$C_T = \frac{T}{\frac{1}{2}\rho U_\infty^2 \pi \sigma_{\text{ad}}^2}, \quad C_P = \frac{P}{\frac{1}{2}\rho U_\infty^3 \pi \sigma_{\text{ad}}^2}, \quad \eta = \frac{C_T}{C_P},$$

where T is the thrust experienced by the rotor, P is the power transferred by the propeller to the fluid and η is the propulsive efficiency. On inspecting Table 2, it is immediately apparent that the errors are monotone decreasing functions of the refinement parameters which are simultaneously increased from SA–1 to SA–6. Furthermore, from a practical point of view, it should be observed that the error magnitude, even for the coarsest combination of

Table 1. SA-ADM: run matrix.

Case no.	n_z	n_{zs}	n_{rs}	*quad_err*	*res*	N	$\hat{b}$	J
SA–1	51	11	11	10^{-5}	10^{-4}	3	10.0	0.5
SA–2	101	51	51	10^{-5}	10^{-4}	3	10.0	0.5
SA–3	201	101	101	10^{-6}	10^{-5}	4	10.0	0.5
SA–4	301	151	151	10^{-6}	10^{-5}	4	10.0	0.5
SA–5	401	201	201	10^{-7}	10^{-6}	5	10.0	0.5
SA–6	501	251	251	10^{-7}	10^{-6}	5	10.0	0.5

Table 2. Error analysis for the SA-ADM.

	Relative errors			L^2 error		
Case no.	C_T	C_P	η	$u\|_{\zeta=-1}$	$u\|_{\zeta=0}$	$u\|_{\zeta=1}$
SA–1	1.187×10^{-2}	1.989×10^{-2}	7.862×10^{-3}	3.342×10^{-3}	2.515×10^{-2}	2.207×10^{-2}
SA–2	9.980×10^{-4}	6.292×10^{-4}	3.685×10^{-4}	3.867×10^{-4}	2.682×10^{-3}	4.057×10^{-3}
SA–3	2.331×10^{-4}	2.069×10^{-4}	2.619×10^{-5}	3.657×10^{-5}	4.901×10^{-4}	2.194×10^{-4}
SA–4	1.226×10^{-4}	1.023×10^{-4}	2.026×10^{-5}	2.388×10^{-5}	1.246×10^{-4}	4.347×10^{-5}
SA–5	1.201×10^{-5}	2.319×10^{-6}	1.433×10^{-5}	4.760×10^{-7}	4.166×10^{-5}	9.712×10^{-6}
SA–6	0	0	0	0	0	0

the numerical parameters, is comfortably small (less than 1% for SA–1 on the propulsive efficiency).

3.2. Grid convergence analysis for the CFD-ADM

The CFD suite Fluent® is a general purpose and widespread analysis software that can handle a variety of complex problems. In particular, it is possible to activate, in a disc shaped region, the source terms in the axial and tangential momentum equations to simulate the presence of the rotor.

With this aim, a 2D computational domain is generated (see Figure 3) and discretized through a structured mesh. The domain is bounded by an inlet and an outlet boundary placed at $\mp 25\sigma_{\text{ad}}$ from the plane of the disc, and by an upper wall located at $50\sigma_{\text{ad}}$ from the ζ-axis. At the inlet a uniform axial velocity U_∞ is imposed, whereas the outlet is treated as a fully-developed flow boundary. An inviscid wall treatment is used for the upper surface. Finally, the axial and the tangential body-force radial profiles, obtained for the reference case SA–6, are prescribed at the actuator disc plane as source terms in the momentum equations. In particular, the computational domain is subdivided into an inner and an outer domain. The first one is the $10\sigma_{\text{ad}} \times 3\sigma_{\text{ad}}$ region around the propeller (see Figure 3) and it is characterized by a uniform density of the mesh. To reduce the computational cost, in the outer domain the density of the mesh is gradually decreased going away from the inner domain. The effects

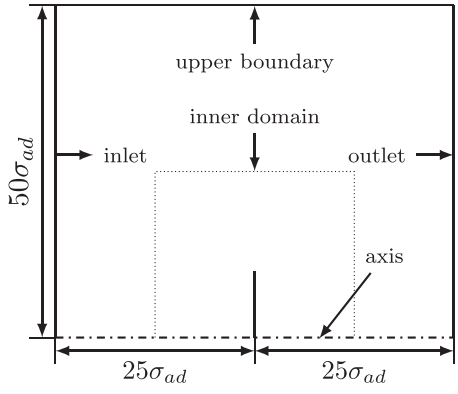

Figure 3. Computational domain (not to scale).

Table 3. Features of the inner domain grid for the CFD error analysis.

Case no.	h	No. of cells
CFD–1	0.08	4,320
CFD–2	0.04	17,280
CFD–3	0.02	69,120
CFD–4	0.01	276,480

of the extension of the inner and outer domains are also investigated through a separate study whose results are omitted for the sake of briefness. The Euler equations are solved employing the well-known SIMPLE algorithm and a second-order discretization scheme. A grid convergence analysis is carried out employing four different structured meshes with an increasing number of nodes (see Table 3). In more detail, the uniform discrete spacing h of the inner domain mesh is doubled moving from the coarser case (CFD–1) to the finer one (CFD–4). Consequently, the number of cells quadruples at each grid level. The relative errors in the performance coefficients and the discrete L^2 errors in u, v and w are shown in Figure 4, where the CFD–4 solution is assumed as reference. The overall trend of the grid convergence study is more than satisfactory. In fact, the rate of error decay is very close to the theoretical value of two. With only the exception of the thrust coefficient, the mesh density appears adequate for the truncation errors to lie in the so-called asymptotic range.

3.3. Comparison of the results

In this section, the results of the SA-ADM and the CFD-ADM will be compared with each other both in terms of local and global quantities. Obviously, the most refined solutions, i.e. SA–6 and CFD–4, will be employed. Also note that, until now, the SA-ADM has been verified only at downstream infinity (see Conway, 1998) through an asymptotic approach. Hence, the comparison reported hereinafter also aims at verifying the SA-ADM in the whole computational domain.

The analysis begins by looking at Figure 5, which reports the radial profiles of the radial, axial and tangential perturbation velocities evaluated through the

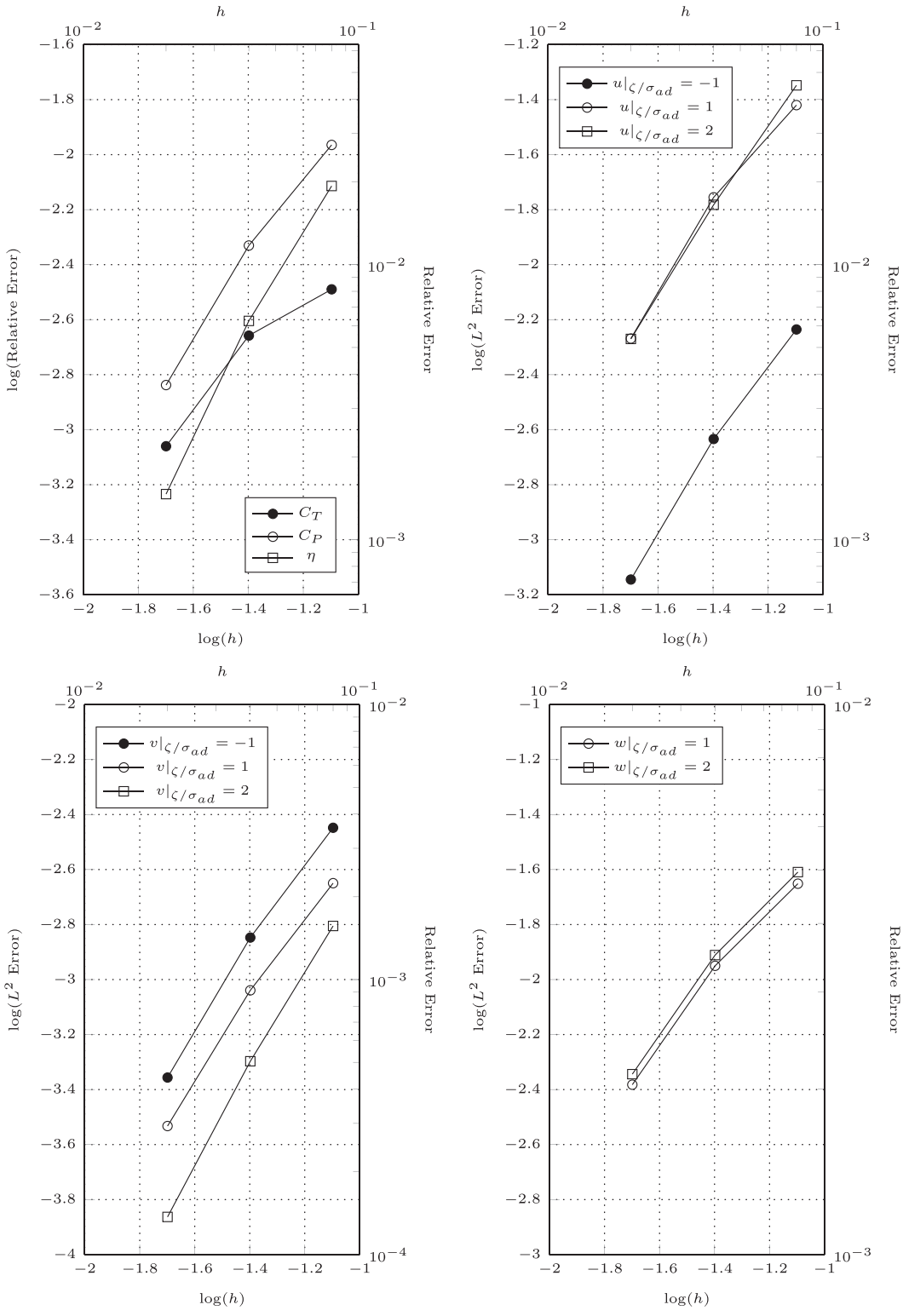

Figure 4. Error analysis for the CFD-ADM.

SA-ADM and the CFD-ADM. As can easily be understood from this figure, the differences between the results of the two methods are extremely small. In particular, no significant differences seem to be present in any velocities components for $\zeta/\sigma_{\text{ad}} = -1$ and $\zeta/\sigma_{\text{ad}} = 1$.

In order to extend the assessment of the two proposed numerical methods to field data, the axial and radial velocity contours are compared in Figure 6. The top half part of the figure shows the contours obtained with the SA-ADM, while the bottom half is related to

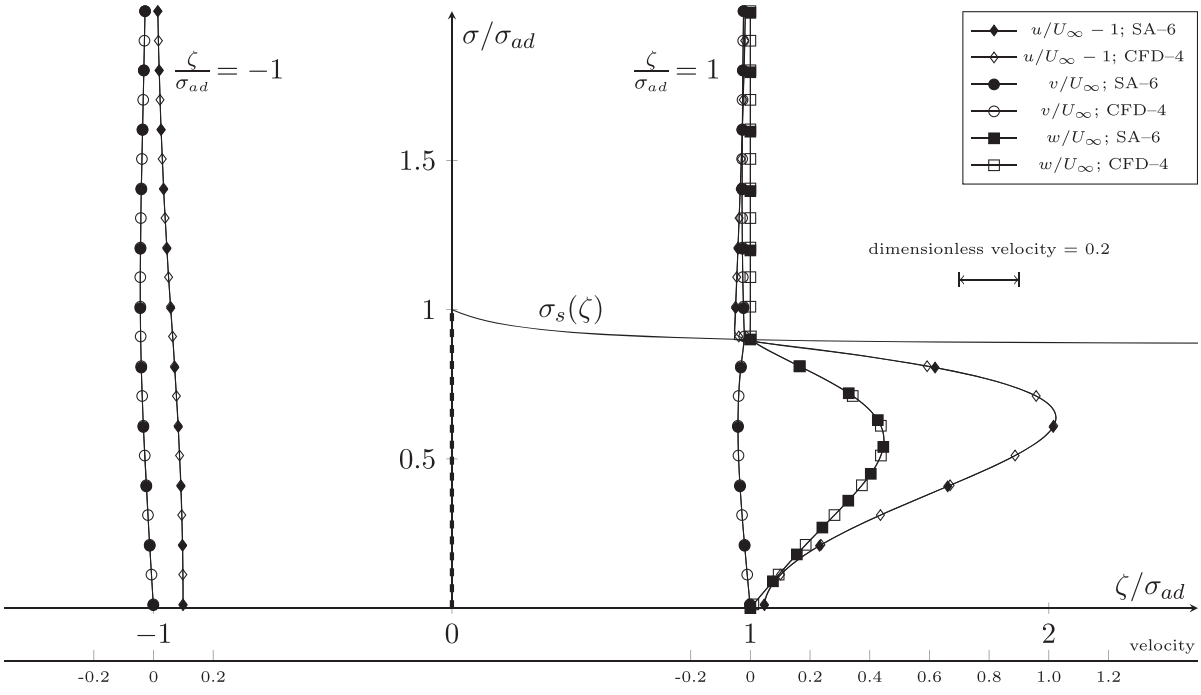

Figure 5. Comparison of the dimensionless velocity for the SA-ADM (SA–6) and CFD-ADM (CFD–4).

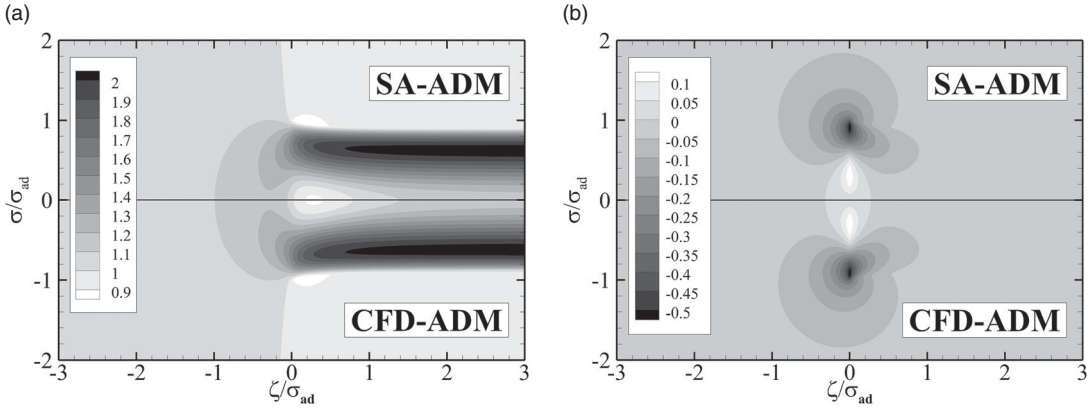

Figure 6. Comparison of the axial (a) and radial (b) velocity contours for the SA-ADM (top) and the CFD-ADM (bottom).

the CFD-ADM. Figure 7 reports the traces in the (ζ, σ)-plane of the streamlines. Moreover, Figure 7 also highlights the possibility of fully taking into account the wake contraction through the SA-ADM. The last two Figures 6 and 7 show that the agreement between the two methods is extremely good in the whole domain. However, some small differences also appear, especially in the proximity of the wake edge. This discrepancy can easily be detected by looking at the shape of the axial velocity iso-line $u/U_\infty = 0.9$ in the wake edge region.

To highlight these aspects further, Figure 8 reports a close-up view of the axial velocity radial distributions for different axial stations. As clearly shown, the discontinuity in the radial derivative of the axial velocity, which takes place at the wake edge, is smoothed in the CFD-ADM; a phenomenon whose impact on the solution could be relieved by locally refining the mesh.

Finally, in Table 4, the differences between the two methods are presented in a quantitative fashion both in terms of performance coefficients and velocity components.

From the wide comparison carried out between the SA-ADM and the CFD-ADM it can be concluded that the agreement between the two methods is excellent in the whole computational domain. This means that they could be used equivalently in the analysis of propellers. However, the methods are obviously characterized by very different computational costs; a fact that makes the

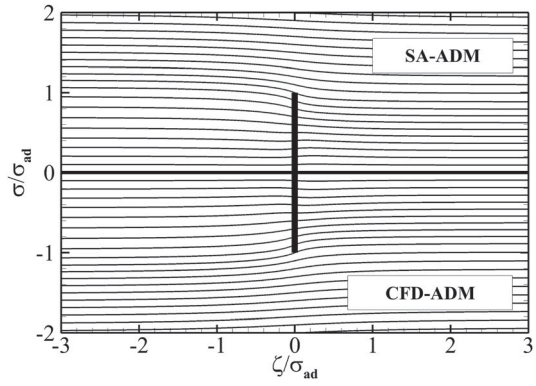

Figure 7. Comparison of the streamline traces for the SA-ADM (top) and the CFD-ADM (bottom).

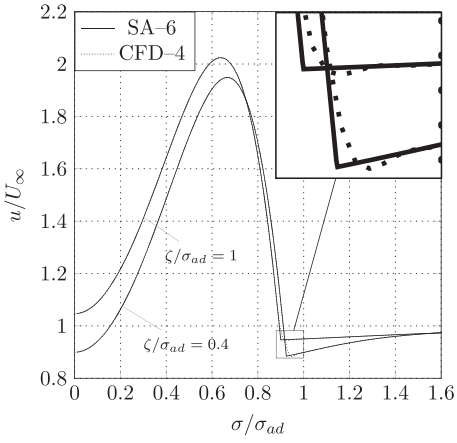

Figure 8. Detailed comparison between SA-ADM (SA–6) and CFD-ADM (CFD–4).

Table 4. Comparison between SA-ADM (SA–6) and CFD-ADM (CFD–4).

		C_T	C_P	η
Relative errors (%)		9.183×10^{-2}	1.282×10^{-1}	3.637×10^{-2}
		$\zeta/\sigma_{ad} = -1$	$\zeta/\sigma_{ad} = 1$	$\zeta/\sigma_{ad} = 2$
L^2 errors	u/U_∞	2.655×10^{-4}	3.981×10^{-3}	3.932×10^{-3}
	v/U_∞	2.589×10^{-4}	1.634×10^{-4}	3.533×10^{-5}
	w/U_∞	–	3.897×10^{-3}	4.254×10^{-3}

SA-ADM extremely attractive for design purposes. This is particularly true in the first stages of a design procedure when a very fast analysis tool is preferable to sweep the design space quickly. The computational cost related to the SA-ADM method is quantified in Figure 9 which, for all cases (see Tables 1 and 3), reports the values of C_P, η and of the CPU time. All simulations have been performed on an Intel® Xeon CPU E5-1620 v2 3.70 GHz.

Figure 9 also shows a shaded area representing a 1% (±0.5%) deviation band from a reference value evaluated as the average of the SA–6 and CFD–4 results. Figure 9 obviously verifies that the computational cost

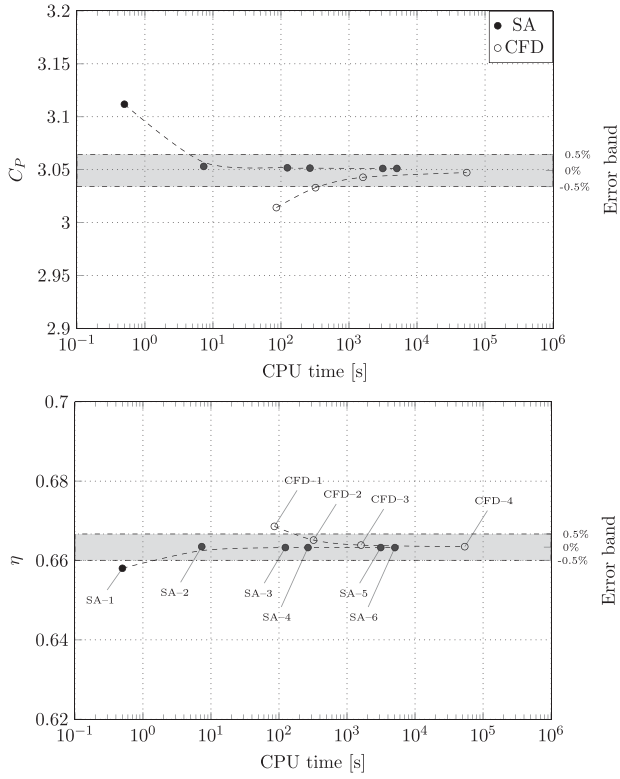

Figure 9. CPU time of the SA-ADM and CFD-ADM.

of the CFD–ADM is bigger than that of the SA–ADM. Moreover, on inspecting these figures it can easily be inferred that, in order to comply with a prescribed accuracy of ±0.5%, the solution SA–2 should be selected for the SA-ADM. The run time of this SA–2 case is seven seconds, a value that can be considered small enough for a preliminary design procedure.

4. Conclusions

This paper has presented the application of the SA-ADM to the analysis of marine propellers. Although the method relies on the simplified assumptions of axisymmetric and inviscid flow regimes, it still provides significant improvements when compared to the widely employed momentum theory or to less advanced actuator disc models available in the literature. Most noticeably, the method allows the convergence of the wake to be accounted for, an important feature that is disregarded in all linear approaches. Additional properties concern the ability of the method to deal with heavy loads of arbitrary radial distribution.

The method has been applied to propellers characterized by a parabolic load distribution whose performance, both in terms of global and local parameters, is compared with those obtained through a CFD actuator disc model. The latter method, which is frequently used to

analyse the flow around marine propellers, represents the effects of the impeller through a set of axisymmetric body forces. The comparison relies on a thorough analysis of the errors of the two methods providing a set of reference solutions characterized by a controlled accuracy. An excellent agreement has been documented between the results of the two methods while the computational complexity is obviously very different. For these reasons, the semi-analytical method is the ideal candidate tool to be adopted in a preliminary design procedure based on the repeated analysis scheme. Furthermore, the collected data may be of interest for the in-depth verification of other numerical approaches.

Ongoing research deals with the assessment of the performance of the method when an arbitrarily shaped hub is introduced. The coupling of the SA procedure with a blade resolving modulus providing the propeller load is also envisaged.

Disclosure statement

No potential conflict of interest was reported by the authors.

ORCID

R. Bontempo http://orcid.org/0000-0001-8087-5111
M. Manna http://orcid.org/0000-0002-2018-7031

References

Basset A. B. (1888). *A treatise on hydrodynamics* (vol. II). London: Deighton Bell.

Bellary S. A. I., Adhav R., Siddique M. H., Chon B. H., Kenyery F., & Samad A. (2016). Application of computational fluid dynamics and surrogate-coupled evolutionary computing to enhance centrifugal-pump performance. *Engineering Applications of Computational Fluid Mechanics*, *10*(1), 172–182.

Bontempo R. (2014). *The nonlinear actuator disk as applied to open and ducted rotors*. Doctoral dissertation, University of Naples Federico II. Retrieved from http://www.fedoa.unina.it/9919/

Bontempo R., Cardone M., & Manna M. (2016). Performance analysis of ducted marine propellers. Part I – Decelerating duct. *Applied Ocean Research*, *58*, 322–330.

Bontempo R., Cardone M., Manna M., & Vorraro G. (2014). Ducted propeller flow analysis by means of a generalized actuator disk model. *Energy Procedia*, *45*, 1107–1115. Retrieved from http://www.sciencedirect.com/science/article/pii/S1876610214001179

Bontempo R., Cardone M., Manna M., & Vorraro G. (2015a). A comparison of nonlinear actuator disk methods for the performance analysis of ducted marine propellers. *Proceedings of the Institution of Mechanical Engineers, Part A: Journal of Power and Energy*, *229*(5), 539–548.

Bontempo R., Cardone M., Manna M., & Vorraro G. (2015b). A comparison of nonlinear actuator disk methods for the performance analysis of ducted marine propellers. In *Proceedings of the 11th European turbomachinery conference*, 23–27 March 2015, Madrid, Spain. Retrieved from http://pia.sagepub.com/content/229/5/539

Bontempo R., & Manna M. (2013). Solution of the flow over a non-uniform heavily loaded ducted actuator disk. *Journal of Fluid Mechanics*, *728*, 163–195. Retrieved from http://journals.cambridge.org/article_S0022112013002577

Bontempo R., & Manna M. (2014). Performance analysis of open and ducted wind turbines. *Applied Energy*, *136*, 405–416. Retrieved from http://www.sciencedirect.com/science/article/pii/S0306261914009842

Bontempo R., & Manna M. (2016a). Analysis and evaluation of the momentum theory errors as applied to propellers. *AIAA Journal*. Retrieved from http://arc.aiaa.org/doi/abs/10.2514/1.J055131

Bontempo R., & Manna M. (2016b). Effects of duct cross section camber and thickness on the performance of ducted propulsion systems for aeronautical applications. *International Journal of Aerospace Engineering*, *2016*, Article ID 8913901. doi:10.1155/2016/8913901

Bontempo R., & Manna M. (2016c). Effects of the duct thrust on the performance of ducted wind turbines. *Energy*, *99*, 274–287.

Bontempo R., & Manna M. (2016d). A nonlinear and semi-analytical actuator disk method accounting for general hub shapes. Part I – Open rotor. *Journal of Fluid Mechanics*, *792*, 910–935.

Breslin J. P., & Andersen P. (1994). *Hydrodynamics of ship propellers*. Cambridge, UK: Cambridge University Press.

Broglia R., Dubbioso G., Durante D., & Di Mascio A. (2013). Simulation of turning circle by CFD: Analysis of different propeller models and their effect on manoeuvring prediction. *Applied Ocean Research*, *39*, 1–10.

Choi J. E., Min K. S., Kim J. H., Lee S. B., & Seo H. W. (2010). Resistance and propulsion characteristics of various commercial ships based on CFD results. *Ocean Engineering*, *37*(7), 549–566.

Conway J. T. (1998). Exact actuator disk solutions for non-uniform heavy loading and slipstream contraction. *Journal of Fluid Mechanics*, *365*, 235–267.

Dai C. M., Gorski J. J., & Haussling H. J. (1991). Computation of an integrated ducted propulsor/stern performance in axisymmetric flow. In *Propellers/Shafting '91 symposium*, 17–18 September 1991, Virginia Beach, VA. Retrieved from https://trid.trb.org/view.aspx?id = 440899

Das S., Bai H., Wu C., Kao J. H., Barney B., Kidd M., & Kuettel M. (2015). Improving the performance of industrial clarifiers using three-dimensional computational fluid dynamics. *Engineering Applications of Computational Fluid Mechanics*, *10*(1), 130–144.

Fu C., Uddin M., & Curley A. (2015). Insights derived from CFD studies on the evolution of planar wall jets. *Engineering Applications of Computational Fluid Mechanics*, *10*(1), 44–56.

Glauert H. (1935). Airplane propellers. In W. F. Durand (Ed.), *Aerodynamic theory* (vol. IV, Division L, pp. 169–360). Berlin: Springer.

Greenberg M. D. (1972). Nonlinear actuator disk theory. *Zeitschrift für Flugwissenschaften*, *20*, 90–98.

Greenberg M. D., & Powers S. R. (1970). *Nonlinear actuator disk theory and flow field calculations, including nonuniform loading* (Contractor Report CR-1672). Washington, DC: NASA.

Greifzu F., Kratzsch C., Forgber T., Lindner F., & Schwarze R. (2015). Assessment of particle-tracking models for dispersed particle-laden flows implemented in openfoam and ANSYS Fluent. *Engineering Applications of Computational Fluid Mechanics*, *10*(1), 30–43.

Hansen M. O. L., Sørensen J. N., Voutsinas S., Sørensen N., & Madsen H. A. (2006). State of the art in wind turbine aerodynamics and aeroelasticity. *Progress in Aerospace Sciences*, *42*(4), 285–330.

Hoekstra M. (2006). A RANS-based analysis tool for ducted propeller systems in open water condition. *International Shipbuilding Progress*, *53*(3), 205–227.

Hough G. R., & Ordway D. E. (1964). The generalized actuator disk. *Developments in Theoretical and Applied Mechanics*, *2*, 317–336.

Hu P., Li Y., Han Y., Cai S. C. S., & Xu X. (2016). Numerical simulations of the mean wind speeds and turbulence intensities over simplified gorges using the SST k–ω turbulence model. *Engineering Applications of Computational Fluid Mechanics*, *10*(1), 361–374.

Insinna M., Griffini D., Salvadori S., & Martelli F. (2014). Conjugate heat transfer analysis of a film cooled high-pressure turbine vane under realistic combustor exit flow conditions. In *ASME Turbo Expo 2014: Turbine technical conference and exposition*, 16–20 June 2014, Düsseldorf, Germany.

Kawamura T., Miyata H., & Mashimo K. (1997). Numerical simulation of the flow about self-propelling tanker models. *Journal of Marine Science and Technology*, *2*(4), 245–256.

Lamb H. (1932). *Hydrodynamics*. Cambridge, UK: Cambridge University Press.

Liu Z., Fang Y., Song A., Xu L., Wang X., Zhou L., … Zhang W. (2015). A multi-domain decomposition strategy for the lattice Boltzmann method for steady-state flows. *Engineering Applications of Computational Fluid Mechanics*, *10*(1), 72–85.

Luo K., Yu H., Dai Z., Fang M., & Fan J. (2016). CFD simulations of flow and dust dispersion in a realistic urban area. *Engineering Applications of Computational Fluid Mechanics*, *10*(1), 229–243.

Lyness J. N. (1970). Algorithm 379: SQUANK (Simpson quadrature used adaptivity-noise killed). *Communications of the ACM*, *13*(4), 260–262. Retrieved from https://dx.doi.org/10.1145/362258.362289

Manna M., Benocci C., & Simons E. (2005). Large eddy simulation of turbulent flows via domain decomposition techniques. Part 1: Theory. *International Journal for Numerical Methods in Fluids*, *48*(4), 367–395.

Manna M., Vacca A., & Deville M. O. (2004). Preconditioned spectral multi-domain discretization of the incompressible Navier–Stokes equations. *Journal of Computational Physics*, *201*(1), 204–223.

Masson C., Ammara I., & Paraschivoiu I. (1997). An aerodynamic method for the analysis of isolated horizontal-axis wind turbines. *International Journal of Rotating Machinery*, *3*(1), 21–32.

Mikkelsen R., Sørensen J. N., & Shen W. Z. (2001). Modelling and analysis of the flow field around a coned rotor. *Wind Energy*, *4*(3), 121–135.

Miyata H., Zhu M., & Watanabe O. (1992). Numerical study on a viscous flow with free-surface waves about a ship in steady straight course by a finite-volume method. *Journal of Ship Research*, *32*(4), 332–345.

Montis M., Niehuis R., Guidi M., Salvadori S., Martelli F., & Stephan B. (2009). Experimental and numerical investigation on the influence of trailing edge bleeding on the aerodynamics of an NGV cascade. In *ASME Turbo Expo 2009: power for land, sea, and air*, 8–12 June 2009, Orlando, FL (pp. 1063–1073).

Nakatake K. (1989). On ship hull–propeller–rudder interactions (in Japanese). In *Proceedings of the 3rd JSPC symposium on flows and forces of ships* (pp. 231–259). Tokyo: The Society of Naval Architects of Japan.

Phillips A. B., Turnock S. R., & Furlong M. (2009). Evaluation of manoeuvring coefficients of a self-propelled ship using a blade element momentum propeller model coupled to a Reynolds averaged Navier–Stokes flow solver. *Ocean Engineering*, *36*(15), 1217–1225.

Piquet J., Queutey P., & Visonneau M. (1987). Computation of viscous flows past axisymmetric bodies with and without a propeller in operation. *Numerical Methods in Laminar and Turbulent Flow*, *5*, 644–655.

Schetz J. A., & Favin S. (1977). Numerical solution for the near wake of a body with propeller. *Journal of Hydronautics*, *11*(4), 136–141.

Schetz J. A., & Favin S. (1979). Numerical solution of a body–propeller combination flow including swirl and comparisons with data. *Journal of Hydronautics*, *13*(2), 46–51.

Shen W. Z., Sørensen J. N., & Mikkelsen R. (2005). Tip loss correction for actuator/Navier–Stokes computations. *Journal of Solar Energy Engineering*, *127*(2), 209–213.

Shi Y., Xu G., & Wei P. (2016). Rotor wake and flow analysis using a coupled Eulerian–Lagrangian method. *Engineering Applications of Computational Fluid Mechanics*, *10*(1), 386–404.

Sørensen J. N. (2011). Aerodynamic aspects of wind energy conversion. *Annual Review of Fluid Mechanics*, *43*, 427–448.

Sørensen J. N., & Kock C. W. (1995). A model for unsteady rotor aerodynamics. *Journal of Wind Engineering and Industrial Aerodynamics*, *58*(3), 259–275.

Sørensen J. N., Shen W. Z., & Munduate X. (1998). Analysis of wake states by a full-field actuator disc model. *Wind Energy*, *1*(2), 73–88.

Starke B., & Bosschers J. (2012). Analysis of scale effects in ship powering performance using a hybrid RANS–BEM approach. In *Proceedings of 29th symposium on naval hydrodynamics (ONR)*, Gothenburg, Sweden, August 2012.

Sun Y., Su Y., Wang X., & Hu H. (2016). Experimental and numerical analyses of the hydrodynamic performance of propeller boss cap fins in a propeller–rudder system. *Engineering Applications of Computational Fluid Mechanics*, *10*(1), 145–159.

Troldborg N., Sørensen N. N., Réthoré P. E., & van der Laan M. P. (2015). A consistent method for finite volume discretization of body forces on collocated grids applied to flow through an actuator disk. *Computers & Fluids*, *119*, 197–203.

Wu T. Y. (1962). Flow through a heavily loaded actuator disc. *Schiffstechnik*, *9*, 134–138.

Yang C., Hartwich P., & Sundaram P. (1991). A Navier–Stokes solution of hull–ring wing–thruster interaction. In *Proceedings of the eighteenth symposium on naval hydrodynamics*, 19–24 August 1990, Ann Arbor, MI. Washington, DC: National Academy Press. Retrieved from https://www.nap.edu/read/1841/chapter/54